JOURNAL OF SOLID STATE CHEMISTRY 11, 94–105 (1974)

Structural Relationships and Mechanisms for the Stoichiometry Change from MX_3 (YF_3-Type) through MX_2 (Fluorite-Type) to M_2X_3 (C-Type Sesquioxide)

A. W. MANN*

School of Physical Sciences, The Flinders University of South Australia, Bedford Park, S.A. 5042, Australia

Received November 7, 1973

Structures produced by inducing stoichiometry changes in crystalline fluorides and oxide–fluorides of yttrium by pyrohydrolysis have been studied by X-ray powder diffraction and electron microscopy. The structures of YF_3, various fluorite-related intermediates and the ultimate product of hydrolysis, Y_2O_3, are all closely related. The pyrohydrolysis is topotactic; the anion sublattice remains intact and vacancies and oxygen substitute for fluorine on the anion sublattice in an ordered, cooperative way to produce fully ordered product structures. A 'unit slip' mechanism, involving the most favourable slip systems for a primitive cubic sublattice, $\langle 001 \rangle \{110\}$ and $\langle 100 \rangle \{001\}$, is postulated as a possible mechanism for the process.

Introduction

Continuous topological variation of coordination in crystals and structural relations between the structure types TiO_2 (rutile), α-PbO_2, and CaF_2 (fluorite) have recently been proposed (*1*). Other structural relationships, involving the concept of crystallographic shear (CS), between structure types of widely differing stoichiometry, α-UO_3, CaF_2, La_2O_3, and NaCl, have also recently been outlined by Hyde (*2*). Prior to this, the concept of CS had been used to explain the accommodation of smaller stoichiometry changes in compounds structurally related to ReO_3 (*3, 4*) and to rutile (*5, 6*) and mechanisms for the production of these CS planes have been proposed by Gado (*7*), Anderson and Hyde (*8, 9*), and Andersson and Wadsley (*10*). These models described the removal of anions from the crystal to produce vacancy planes on the anion sublattice, and the subsequent collapse and shear (CS) of the entire structure across this vacancy plane. It appears, however, in certain structure types, particularly those related to the fluorite-type, that the CS mechanism does not operate, and relationships between structures differing in stoichiometry exist for which one sublattice remains intact. This paper reports the observations of some large stoichiometry changes induced in fluorite-related structures at temperatures where the anion sublattice alone is mobile.

Large deviations from MX_2 stoichiometry, involving either anion excess or anion deficiency, can be tolerated by the fluorite structure. Ordered phases conforming to a general homologous series M_nO_{2n-2} have been observed in the PrO_x (*11*) and CeO_x (*12*) ($1.5 < x < 2.0$) systems. Mixed oxides of the type MO_2 (fluorite)–M_2O_3, e.g., ZrO_2–Sc_2O_3, produce intermediate phases which are superstructures of the fluorite type with ordered arrangements of anion vacancies (*13*). Ordering of excess oxygen in the fluorite-type structure of UO_2 results in the superstructure phase U_4O_9 (*14*); here the interstitial oxygens are located in specific sites in the distorted fluorite structure. The oxide–fluoride, M_2O_3–MF_3 (M = yttrium or rare-earth cation),

* Present address: CSIRO, Division of Mineralogy, Private Mailbag, P.O., Wembley, W.A. 6014.

systems have been shown to form superstructures based on ordering of interstitial anions in the fluorite structure. In the Y_2O_3–YF_3 system (*15*, *16*), the composition region $YX_{2.13}$–$YX_{2.22}$(X = O + F) reveals a large number of extremely closely related "ordered intergrowth" phases; these phases are intergrowths of two adjacent members of the homologous series $Y_nO_{n-1}F_{n+2}$(n = 4, 5, 6, 7, 8) and have interstitial anions ordered on planes parallel to $(010)_F$[1] and separated by $n/2$ fluorite subcell units. The sequence of spacings generated by the interstitial layers determines the average length of the unit cell, which has been observed to be as large as 317Å. The fluorite structure is also capable of accommodating deviations from MX_2 stoichiometry in a disordered manner. At high temperatures in the PrO_x (*11*), CeO_x, and mixed oxide systems (*13*) a cubic (α) phase exists and Roether (*17*) has also reported a cubic (α) form for various oxide–fluorides at higher temperatures. Clearly, for these latter examples, a mobile anion sublattice is required, on which the vacancies or interstitials can be randomized.

The low temperature phases of the YF_3–Y_2O_3 system have been studied in some detail (*15*, *16*, *18*). Four broad phase types are observed; YF_3, "orthorhombic phases," YOF, and Y_2O_3. YF_3 is orthorhombic and stoichiometric. The "orthorhombic phases" are the sequence of fluorite related superstructure phases occurring in the composition region $YX_{2.13}$–$YX_{2.22}$. Stoichiometric YOF is hexagonal (rhombohedral) with a slightly distorted fluorite structure, and Y_2O_3 has the cubic C-type sesquioxide (bixbyite) structure. At other compositions diphasic mixtures of these phases exist at low temperatures.

Zachariasen (*15*) first described the hydrolysis of YF_3, which he used as a preparative and analytical technique, in a crystal chemical examination of phases in the YF_3–Y_2O_3 system. The phases obtained on heating YF_3 were:

YF_3 + tetragonal YOF[2] (after 24 hr at 400°C);
tetragonal YOF (after 48 hr at 500°C);
rhombohedral YOF + tetragonal YOF (after 72 hr at 500°C);
rhombohedral YOF (after 96 hr at 500°C);
Y_2O_3 (after 48 hr at 900°C).

The stoichiometry changes described in this paper, produced by heating crystals under low vacuum conditions with only traces of water vapour present, are thought to have occurred by this mechanism. The reaction for pyrohydrolysis of an oxide–fluoride of composition MX_a (where 'a' is the number of anions per cation), i.e., $MO_{3-a}F_{2a-3}$, is:

$$MX_a + xH_2O \rightarrow MX_{a-x} + 2xHF$$

or

$$MO_{3-a}F_{2a-3} + xH_2O \rightarrow MO_{(3-a+x)}F_{(2a-3-2x)} + 2xHF$$

To preserve charge neutrality, each reactant water molecule must replace two fluoride ions by an oxide ion, producing a decrease in the overall anion to cation ratio.

Experimental Methods

Methods used for sample preparation and analysis of yttrium oxide–fluorides have been described in an earlier publication (*16*). Two of these samples, annealed YF_3 and sample $YX_{2.18(3)}$ were chosen for the heating experiments of the present study. A Guinier–Lenné high temperature powder diffraction camera, with focused Cu$K\alpha$ radiation was used to observe the pyrohydrolysis of a powdered $YX_{2.18(3)}$ sample. The camera was programmed for a heating rate of approximately 12°/hr, and a film traverse speed of 2 mm/hr. A pressure of approximately 10^{-3} Torr was maintained in the camera throughout the heating cycle. Crushed samples of both YF_3 and $YX_{2.18(3)}$ were examined in an AEI EM802 electron microscope fitted with a goniometer stage and high tilt cartridge, and operated at 100 kV. Pulse heating of small crystals was carried out using either the beam current and condenser lens controls, or by momentarily removing the condenser aperture

[1] The subscript F refers to the fluorite-type sub cell.
[2] "Tetragonal YOF" was the early description for the "orthorhombic phases" (see Ref. *16*).

at low beam current values. The operating pressure of the microscope, measured directly above the diffusion pump, during the experiment was not greater than 10^{-5} Torr.

Results

Guinier–Lenné Camera Pyrohydrolysis Experiment

Part of the diffraction pattern recorded for the pyrohydrolysis of $YX_{2.18(3)}$ powder is shown in Fig. 1.

Strong fluorite-type reflections and some superstructure reflections for the orthorhombic phase $YX_{2.18(3)}$ were evident prior to commencement of the heating cycle (these are marked "O" at the top of Fig. 1). Pyrohydrolysis proceeded as the temperature was raised, and at a time–temperature relationship (i.e., composition of sample) corresponding to attainment of a temperature of 200°C, diffraction lines of a second phase, hexagonal YOF ("H") appeared. Reflections indicative of a disordered cubic phase were not at this stage evident.

Hexagonal YOF lines "H" were joined by an addition reflection at the $\{220\}_F$ position (marked as "T" in Fig. 1) at a temperature (and composition) corresponding to approximately 240°C. This line is an indication of an important phase (or phases) which does not exist at room temperature in the Y–O–F system, but does have an analogue at room temperature in the Yb–O–F system. This phase will be discussed in detail later. As the pyrohydrolysis proceeded, bcc lines of C-type Y_2O_3 ,"Y", appeared[3] *before* hexagonal YOF was converted to a disordered fcc fluorite phase "F", the latter occurring at a temperature (and composition) corresponding to approximately 265°C. The final step in the pyrohydrolysis was conversion of this fcc phase to bcc Y_2O_3.

Electron Microscope Heating Experiments

(*a*) *Pyrohydrolysis of YF_3 crystals.* Figures 2a and 2b are the {011} zone axis electron

[3] Not clearly evident on the reproduction in Fig. 1 but apparent, particularly at $\{111\}_F$, on the original.

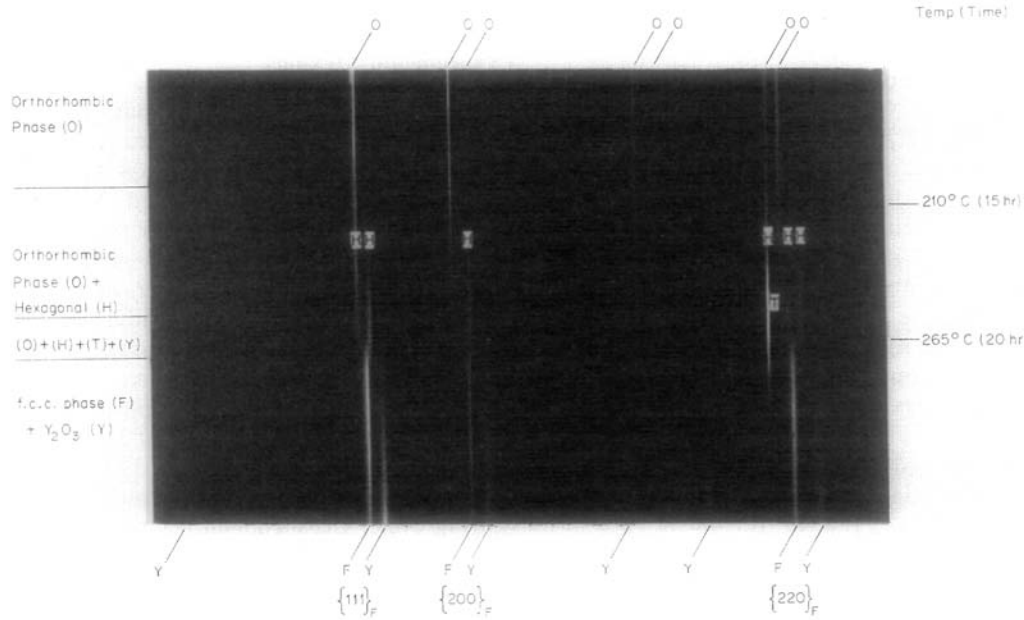

FIG. 1. Guinier–Lenné powder camera diffraction record of the pyrohydrolysis of $YX_{2.18}$–Y_2O_3. The phases present are indicated down the left hand side, and the temperatures and total heating times down the right hand side.

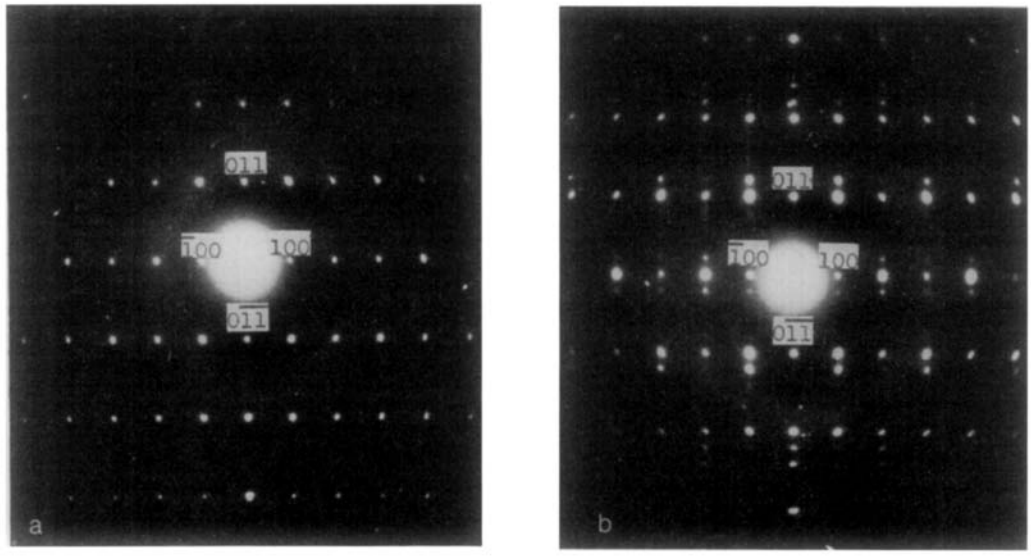

FIG. 2. The [01$\bar{1}$] zone axis diffraction pattern of a YF_3 crystal (a) before pulse heating and (b) after pulse heating in the electron microscope. The composition of the crystal in Fig. 2b is approximately $YX_{2.20}$.

diffraction patterns of a YF_3 crystal before and after pulse heating with the electron beam of the microscope. Less than 0.5° of tilt was required after heating to obtain the oriented pattern of Fig. 2b and an orientational relationship between the two patterns was evident. The pattern in Fig. 2b is very similar to those obtained from samples in the Nd–O–F system in the anion excess region from $NdX_{2.18}$ to $NdX_{2.35}$ (*19*); the patterns arise from superstructures of fluorite with interstitial anions ordered onto $(110)_F$ planes. These are designated "Z" phases after Zachariasen who first recognized the tetragonal subcell, $\sqrt{2}a_F/2 \times \sqrt{2}a_F/2 \times a_F$. The pattern in Fig. 2b is that from a unit cell $(5 \times 1 \times 1)$ of these "Z" subcell units. The most likely composition for this phase, by analogy with the neodymium phases, is $(Y_5O_4F_7)_2(=YX_{2.20})$; the phase will be designated $YX_{2.20}(Z)$. It is not the equilibrium room temperature phase for this composition in the YF_3–Y_2O_3 system. Attempts to "anneal" $YX_{2.20}(Z)$ to $YX_{2.20}(O)$, the corresponding orthorhombic phase, were not successful; further strong heating of $YX_{2.20}(Z)$ resulted in crystal fragmentation.

The hydrolysis reaction for the observed stoichiometry change is:

$$5YF_3 + 4H_2O \rightarrow Y_5O_4F_7 + 8HF.$$

(*b*) *Pyrohydrolysis of a* $YX_{2.18(3)}$ *crystal.* Figures 3a–c are the $[100]_F$ zone axis diffraction patterns at various stages of pulse heating a $YX_{2.18(3)}$ crystal. Figure 3a is $[100]_F$ zone axis pattern for the unheated crystal and is identical with that for the room temperature orthorhombic phase at the same composition; the superstructure reflections along $[010]_F$ are seen to be finely split, indicating a large unit cell, 47 fluorite units in fact (*16*). For the purposes of this paper however the exact nature of this phase need not be considered, an idealized 5F or fivefold fluorite unit corresponding to the composition $YX_{2.20}$ can be used.[4] Henceforth, this orthorhombic phase will be designated $YX_{2.20}(O)$. Pulse heating $YX_{2.20}(O)$ produced the fluorite-type $(100)_F$ section of Fig. 3b; other sections for crystals of this phase after pyrohydrolysis indicated that Fig. 3b was in fact a section of the reciprocal lattice appropriate to hexagonal YOF. Figure 3c is a diffraction pattern of the final product of further pulse heating; it is the [100] zone axis diffraction pattern appropriate to C-type Y_2O_3. The intensities of reflections in this pattern are in good qualitative agreement with those described for Y_2O_3 by Paton

[4] The idealization in no way changes the concepts involved.

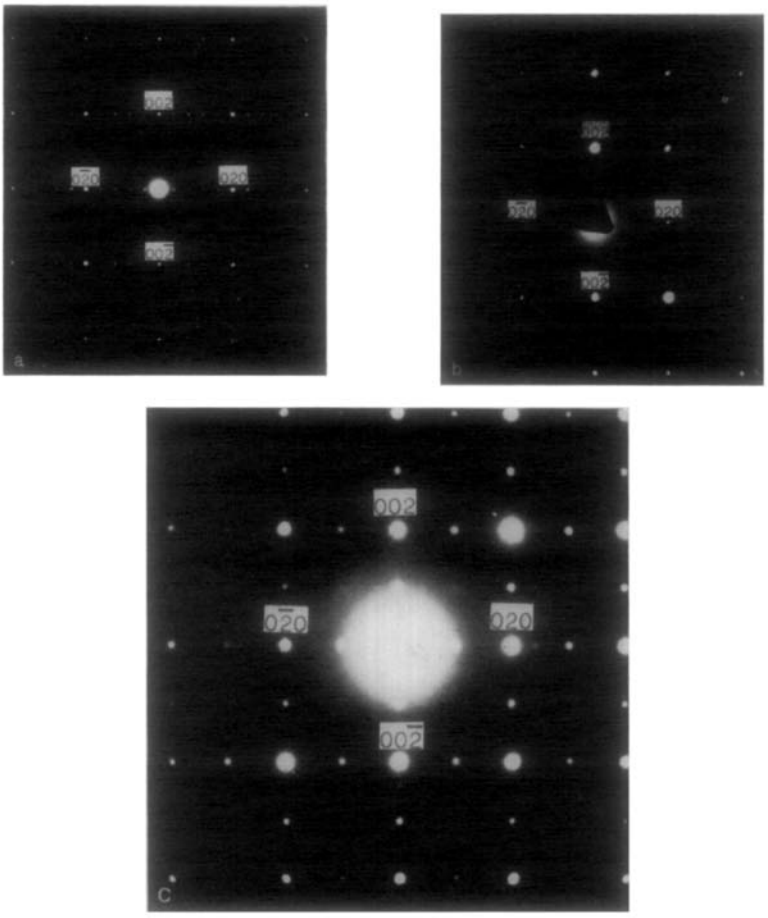

FIG. 3. The $[100]_F$ zone axis patterns of a $YX_{2.18(3)}$ crystal pulse heated in the electron microscope. (a) The unheated crystal. (b) The diffraction pattern (that of YOF) obtained after a short pulse heating. (c) The diffraction pattern (that of Y_2O_3) obtained after prolonged pulse heating.

and Maslen (*20*). No change in orientation of the crystal was necessary to obtain the patterns of Figs. 3b and 3c. Electron micrographs of the specimen crystal before and after heating indicated that no apparent change in crystal morphology had occurred during pyrohydrolysis. The hydrolysis reactions for these stoichiometry changes are:

$$Y_5O_4F_7 + H_2O \rightarrow 5YOF + 2HF$$
$$YOF + \tfrac{1}{2}H_2O \rightarrow YO_{1.5} + HF.$$

(*c*) *Pyrohydrolysis of* $YbX_{1.85}$ *crystal.* The appearance of an additional $\{220\}_F$ reflection marked as "T" in the Guinier–Lenné film (Fig. 1), has already been noted. In the ytterbium oxide–fluoride system an ordered phase at a composition close to $YbX_{1.85}$ (i.e., substoichiometric relative to fluorite) is observed (*21*). The $[1\bar{1}1]_F$ zone axis electron diffraction pattern for a crystal of this phase is shown in Fig. 4a. Here again superstructure (with fine splitting) is evident, this time along $[220]_F$. If the fine splitting and displacement of superstructure reflections are ignored, this pattern and the corresponding powder pattern can be indexed with a superstructure unit cell $(6 \times 1 \times 1)$ times the Zachariasen (Z)-type sub-cell. The idealized formula for this unit is $(Yb_6O_7F_4)_2$ or $YbX_{1.83}$; this idealization will be used for the remainder of the paper. Figure 4b shows the diffraction pattern, a

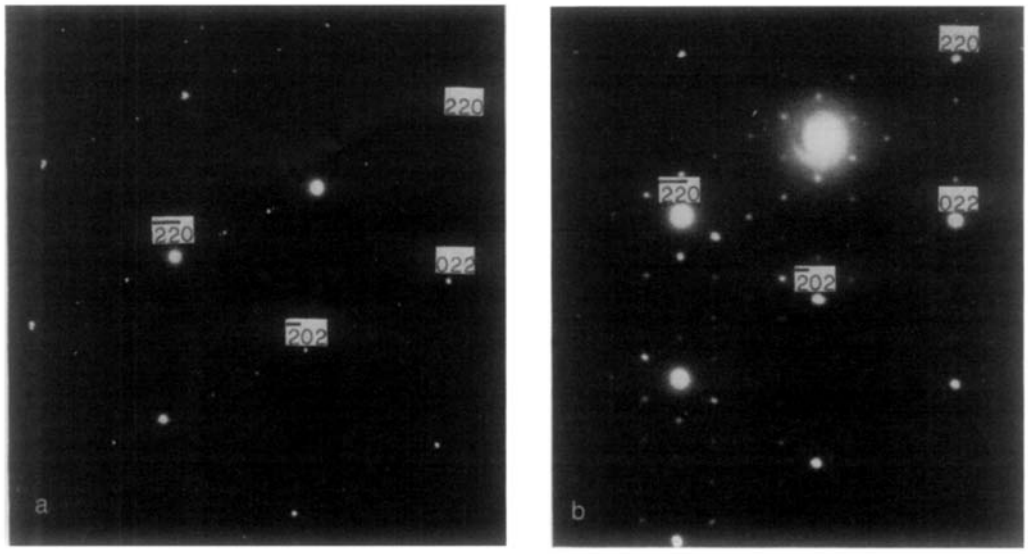

FIG. 4. The [1$\bar{1}$1] zone axis diffraction pattern of a $YbX_{1.85}$ crystal, (a) before pulse heating and (b) after pulse heating in the electron microscope. The diffraction pattern in Fig. 4b is that for a [111] zone axis of Yb_2O_3.

[1$\bar{1}$1] zone axis pattern appropriate to C-type Yb_2O_3, obtained after pulse heating the $YbX_{1.83}$ crystal; once again the orientation of the crystal was not altered during the course of the experiment. The hydrolysis reaction for the stoichiometry change is:

$$Yb_6O_7F_4 + 2H_2O \rightarrow 3Yb_2O_3 + 4HF.$$

Observed orientational relationships. In all of the pyrohydrolysis experiments, specific and reproducible orientational relationships were observed. The indices of some of the equivalent diffraction planes before and after pyrohydrolysis are shown in Table I; in all cases within this table, the diffraction plane indices appropriate to the true unit cell have been used. Observed structural relationships are shown connected by arrows and the direction of each arrow indicates the sense of the pyrohydrolysis reaction producing the stoichiometry change.

Interpretation of Results

1. Relationships Between Reactant and Product Structures

The gross structural features of each of the reactant and product crystals, and the relationships between them, provide some important clues as to the mechanism of pyrohydrolysis; for the preliminary investigation of structural relationships it is convenient to make no distinction between oxygen and fluorine on the anion sublattices.

1(a). Relationship between YF_3 and $YX_{2.20}$ (Z). Hyde (*22*) has formalised the relationship between YF_3 and fluorite; discrete {100} anion rows or "strings" inserted into the latter produce the YF_3 structure. These anion "strings" lie very nearly on (011) planes[5] of the YF_3 structure, as shown by the dotted lines in Fig. 5a.

If the anions on the (011) planes marked "R" in Fig. 5a are removed, a structure very similar to that for $YX_{2.20}$(Z) remains, with interstitial planes "I" parallel to $(110)_F$ in a fluorite matrix and occurring 5 tetragonal subcells apart (see Fig. 5b). The cations and remaining anions of YF_3 are required to undergo only minor positional shifts to reproduce the fluorite-type matrix.

1(b). Relationship between $YX_{2.20}$(O) and YOF. The exact crystal structure for the phase $YX_{2.20}$(O) ($=Y_5O_4F_7$) has not yet been determined. However the full structure of the member $n = 7$, $Y_7O_6F_9$, of the same homolo-

[5] The (011) planes of YF_3 are parallel to $(110)_F$.

TABLE I

SOME OBSERVED DIFFRACTION PLANE EQUIVALENTS BEFORE AND AFTER PYROHYDROLYSIS

Fluorite-type reflection plane	$(00l)_F$	$(0k0)_F$	$(hh0)_F$	$(hhh)_F$
PHASE				
YF_3	(100)		(011)	
$YX_{2.20}(Z)$	(001)		(500)	
$YX_{2.20}(O)$	(002)	(0(10)0)	(220)	(151)
YOF	(104)	($\bar{1}$14)	($\bar{1}$08)	($\bar{1}$02) or (006)
Disordered YOF	$(002)_F$	$(020)_F$	$(220)_F$	$(111)_F$
$YX_{1.83}$	(002)	(610)	((12)00)	(601)
Y_2O_3	(004)	(040)	(440)	(222)

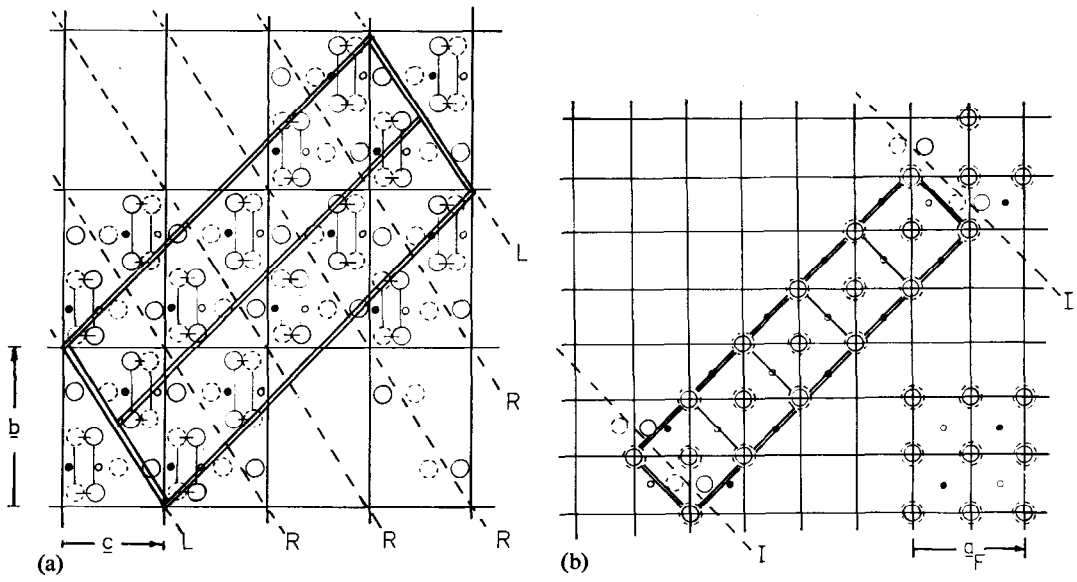

FIG. 5(a). The YF_3 structure projected onto (100). Anions on "R" planes shown in projection as dotted lines, are removed to obtain the structure for $YX_{2.20}(Z)$; two potential unit cells for $YX_{2.20}(Z)$ are shown in double outline. (b). The $YX_{2.20}(Z)$ structure projected onto $(001)_F$; the unit cell is shown in double outline. ● = yttrium at $x \sim 0.25$; ○ = yttrium at $x \sim 0.75$; ○ = fluorine at $x \sim 0.00$; ○ = fluorine at $x \sim 0.50$.

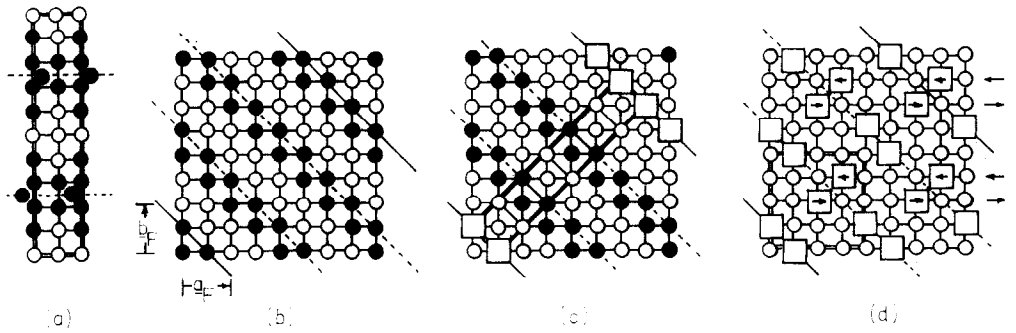

FIG. 6. Projections of idealized anion layers for the following structures onto $(001)_F$. (a) $YX_{2.20}(O)$—the interstitial layers to be removed to obtain YOF are marked as dotted lines. (b) YOF—the fluorine layers to be removed to obtain $YX_{1.83}$ are shown as full lines. (c) $YX_{1.83}$—the fluorine layers, to be removed to obtain Y_2O_3 are shown as dotted lines. (d) Y_2O_3—shifts of vacancies (as planes) to produce $(112)_F$ vacancy planes are arrowed. The projections of unit cells, where appropriate, are shown in double outline. ○: oxygen, ●: Fluorine; □: vacancy.

gous series has been reported (*23*) as has the structure for YOF (*18*). The phase $YX_{2.20}(O)$ has, by analogy with $Y_7O_6F_9$, interstitial anions inserted in layers parallel to (010) and separated by $b/2 = 2\frac{1}{2}$ fluorite unit cells [see Fig. 6a]. One anion layer of the YOF structure is shown in Fig. 6b.[6]

To obtain the fluorite-type YOF structure from $YX_{2.20}(O)$ one formally has only to remove the layers of interstitial anions.

1(c). Relationship between YOF and $YX_{1.83}$. One anion layer of the proposed structure for the substoichiometric phase $YX_{1.83}(=Y_6O_7F_4)$ is shown in Fig. 6c.[7] This arrangement, which has vacancies ordered onto $(110)_F$ planes, can be obtained from the YOF fluorite-type structure by introducing a vacancy plane on every twelfth $(110)_F$ anion plane of YOF, as shown by the full lines on the projection in Fig. 6b.

1(d). Relationship between YOF and C-type Y_2O_3. The basic structural relationship between the C-type sesquioxide and fluorite structures is well known (*24*). Oxygens are missing from across body and face diagonals of fluorite MO_8 cubes to provide the six-fold metal coordination polyhedra of C-type sesquioxides. The observed vacancy arrangement in C-type Y_2O_3 cannot be rationalized in terms of any one simple low index set of planes. The nearest approach to this is shown in Fig. 6d; the broken lines mark the positions of intersection of some $(112)_F$ planes with an $(001)_F$ anion layer.[8] The $(112)_F$ planes marked contain, in the actual structure, oxygens and vacancies; they become vacancy-only planes if the oxygen pairs on them are interchanged with the pairs of immediately adjacent vacancies as indicated by the arrows in Fig. 6d. This idealized structure for Y_2O_3 can be obtained from YOF by introducing vacancies onto every fourth $(112)_F$ plane of YOF shown by the dotted and full lines in Figs. 6b–d.

2. *Possible Reaction Mechanisms*

Reaction mechanisms postulated for the pyrohydrolysis reactions on the basis of the observed stoichiometry changes and orientational relationships between reactant and product can, at this stage, only be proposed tentatively. However, 4 observations within the present series of experiments help to characterize the reaction mechanism:

(1) In all cases the pyrohydrolysis reaction is a topotactic reaction, i.e., an orientational relationship exists between all reactants and products.
(2) These orientational relationships can be directly related to specific structural

[6] Successive $(001)_F$ anion layers of YOF are obtained from the one shown by shifts of $a/2$ [010] or $a/2$ [100]. Fluorines and oxygens are ordered onto $(111)_F$ planes in YOF.

[7] Successive $(001)_F$ anion layers of $YX_{1.83}$ are identical with the one shown.

[8] Successive $(001)_F$ anion layers of Y_2O_3 are obtained from the one shown by successive shifts of a [0$\bar{1}$0].

features, e.g., fluorine planes in reactant crystal or vacancy planes in product crystals.

(3) No disruption of the cation sublattice is observed or required for any stoichiometry or structure change.

(4) In at least one case ($YX_{2.20}(O) \rightarrow$ YOF) "disordering" of the anion sublattice and lowering of the subcell symmetry is not required to achieve stoichiometry change.[9]

These observations are suggestive of cooperative anion movement during pyrohydrolysis, irrespective of whether the actual mechanism involves surface hydrolysis or a hydrolysis reaction occurring in the bulk of the crystal. In either case, the mechanism must provide for explusion of fluoride ions, initially existing on specific anion *planes*, and for their replacement by oxide ions and vacancies, again occurring on specific crystallographic *planes* of the product.

Planar movement of anions is thus both a result of, and a suggestive clue to, the hydrolysis mechanism. Movement of a particular anion plane relative to the remainder of the crystal can be initiated and propagated by movement of individual anion rows or "strings" contained in that crystallographic plane; in turn, the displacement of an anion row relative to the remainder of the crystal can be regarded as the net result of successive cooperative movements of individual anions of that row. The end result in such cases is "slip" of the crystallographic anion plane relative to the remainder of the crystal. This mechanism for movement of individual crystallographic planes of the anion sublattice will be here referred to as "unit slip."

A "unit slip" mechanism based on the available slip systems for a primitive cubic lattice provides a workable reaction mechanism hypothesis for all observed reactions. The favoured slip direction for a primitive cubic array is ⟨001⟩ and the most favourable slip systems are ⟨001⟩{110} and ⟨100⟩{001} (*25*). The favoured slip direction for a primitive cubic array, ⟨001⟩ is particularly relevant to the cooperative movement of anions in fluorite-type structures since:

(a) The fluorite anion sublattice is primitive cubic.

(b) The ⟨011⟩ anion rows of a fluorite array contain no metal atoms.

(c) The distance of closest approach of anion-cation (centre to centre) when an anon string is "pulled" in the ⟨001⟩ direction for a fluorite cell with a_F = 5.40 Å is 1.91 Å, far greater than that for any other direction.

The detailed application of the two slip systems $\langle 001\rangle_F\{110\}_F$ and $\langle 100\rangle_F\{001\}_F$ to the derivation of the pyrohydrolysis structures is shown in Table II.

2(a). Mechanism for the reaction $YF_3 \rightarrow YX_{2.20}(Z)$. Removal of four-fifths of the (011) fluorine-only planes of YF_3 achieves the $YX_{2.20}(Z)$ arrangement (Figs. 5a and b). Although the anion arrangement in YF_3 is not primitive cubic, Fig. 5a reveals that removal of (011) fluorine planes by [100](011) slip might be achieved as easily in YF_3 as in the fluorite structure, for similar reasons (i.e., the [100] anion rows contain no yttrium atoms, etc.). To achieve the composition required for $YX_{2.20}(Z)$, i.e., $Y_5O_4F_7$, some of the additional fluorines of YF_3 must be replaced by oxygens; these same (011) planes of YF_3 are presumably available for the removal of adjacent fluorines from the structure and for their replacement by oxygen during the pyrohydrolysis and alteration of YF_3.

2(b). Mechanism for the reaction $YX_{2.20}(O) \rightarrow YOF$. In a similar way one might expect to derive the YOF fluorite-type structure very simply from $YX_{2.20}(O)$ by removing the appropriate (010) planes of interstitials (see Fig. 6a) by $[100]_F(010)_F$ or $[001]_F(010)_F$ slip. However, these interstitial planes also contain yttrium atoms, and intuitively it seems more likely that 1 in every 5 $(010)_F$ anion planes of the fluorite-type sublattice array (fluorines adjacent to the interstitials) will be removed, by $[100]_F(010)_F$ or $[001]_F(010)_F$ slip, and replaced by oxygens and the interstitial fluorines. The oxygen–fluorine arrangement for YOF

[9] Gross anion sublattice rearrangement, as shown by disintegration of the crystal, was however required to alter the $(110)_F$ distribution of interstitials of $YX_{2.20}(Z)$ to that, $(010)_F$ for $YX_{2.20}(O)$.

TABLE II

DERIVATION OF THE PYROHYDROLYSIS STRUCTURES BY "UNIT SLIP"

Structure	Derived from	Slip system for anion removal	Frequency of removal	Sublattice slip system for "stress relief"	Frequency of relief	Resultant defect plane
$YX_{2.20}(Z)$	YF_3	$[100](011)$	4/5	—	—	(011)
YOF	$YX_{2.20}(O)$	$[001]_F(010)_F$	1/5	—	—	
$YX_{1.83}$	YOF	$[001]_F(110)_F$	1/12	$a/2[0\bar{1}0]_F(001)_F$	3/4	$(110)_F$
Y_2O_3 (idealized)	$YX_{1.83}$	$[001]_F(110)_F$	1/4	$a[010]_F(001)_F$	1/2	$(112)_F$
Y_2O_3 (actual)	$YX_{1.83}$	$[001]_F(110)_F$	1/4	$a[010]_F(001)_F$	1/2	
				and		
				$a/2[100]_F(010)_F$		
				$a/2[\bar{1}00]_F(010)_F$	2/4	—

can only be exactly obtained by allowing rearrangement of the oxygens and fluorines of $YX_{2.20}(O)$ over the fluorite-type sites; although slip mechanisms can be postulated for this, the exact mechanism by which the rearrangement occurs is not yet clear.

2(c). Mechanism for the reaction YOF → $YX_{1.83}$. Oxygens and fluorines are ordered onto $(111)_F$ planes in YOF and these planes occur in pairs (see Fig. 6b). In the $YX_{1.83}$ structure, oxygens, fluorines, and vacancies are ordered onto $(110)_F$ planes (see Fig. 6c). The slip system $[001]_F(110)_F$ can be used to remove fluorines from any one $(001)_F$ layer of YOF (fluorines occur in YOF, as required, on every twelfth $(111)_F$ plane). To remove a complete plane of fluorines from YOF by $[001]_F(110)_F$ slip *and* to achieve ordering of oxygens, fluorines, and vacancies onto $(110)_F$ planes for the product $YX_{1.83}$, successive $(001)_F$ layers of YOF must be "stress relieved" by the slip $a/2[0\bar{1}0]_F(001)_F$. "Stress relief" of a particular $(001)_F$ layer of the crystal may in fact occur as a precursor and prerequisite to the pyrohydrolysis and removal of fluorines from the particular layer; in this case the anion plane removal by $[001]_F(110)_F$ and "relief slip," $a/2[0\bar{1}0]_F(001)_F$ probably occur alternately and proceed through the crystal to remove $(111)_F$ fluorine layers and leave oxygens and vacancies ordered on $(110)_F$ planes.[10]

2(d). Mechanism for the reaction $YX_{1.83}$ → Y_2O_3. The idealized C-type Y_2O_3 structure, with vacancies ordered onto $(112)_F$ planes, can be mechanistically derived from $YX_{1.83}$ by removing all $(110)_F$ fluorine layers from that structure, as shown by the dotted lines in Fig. 6c, and stress relieving, by "unit slip" every second (001) plane using $a[010]_F(001)_F$. Further, all of the vacancies of these idealized $(112)_F$ planes which need to be "relaxed" to obtain the true C-type vacancy configuration, can reach their equilibrium positions by two further (opposing) slips, $a/2[100]_F(010)_F$ and $a/2[\bar{1}00]_F(010)_F$, operating on two out of every four $(010)_F$ anion planes, as shown by the arrows in Fig. 6d.

Discussion

Hyde, Bursill, O'Keeffe, and Anderson (*1*), describe two distinct ways to achieve continuous transformations between the rutile, α-PbO_2 and fluorite structures. The first is a continuous topological homogeneous deformation mechanism, the second a "unit

[10] If removal of entire $(111)_F$ fluorine layers occurred, structure collapse producing CS, as discussed by Hyde (*2*), would occur.

slip" (dislocation/stacking fault) mechanism. The latter is similar to the mechanism proposed in the present case; deformation of the crystals during transformation, implied by the former mechanism, was not observed here. It is of note that $\langle 001 \rangle_F \{110\}_F$ is a recognized slip system for CaF_2 at higher temperatures (*26*).

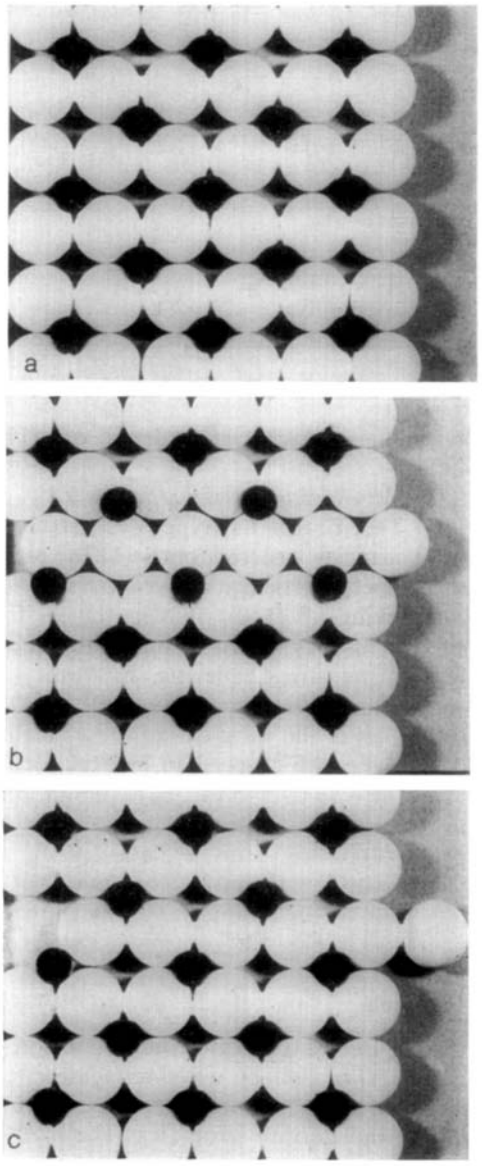

FIG. 7. "Unit slip" of anion sublattice in fluorite-type structure. If cations follow the configuration shown in Fig. 7b the fluorite-type structure shown in Fig. 7a is reproduced as the slip magnitude reaches $a/2[100]_F$ (Fig. 7c).

The anion sublattice modification to the present fluorite-type structures by "unit slip" can in fact be demonstrated by models of fluorite-type $(001)_F$ layers as shown in Fig. 7. As an anion row of fluorite is slipped, each cation has two alternative sites into which to "fall," Movement of cations into one configuration produces α-PbO_2 (Hyde et al. (*1*)); if cations move into sites shown in Fig. 7b the fluorite arrangement is reproduced as the slip magnitude reaches $a/2[100]_F$. Displacement of cations from the fluorite-type sites is minimal throughout the process.

The term "stress relief" has been used in connection with "swinging shear plane" rationalization of the series of structures of general formula Ti_nO_{2n-a} (with n and a integers) related to rutile (*6*). CS operations of the type $\frac{1}{2}[0\bar{1}1]$ (132) were resolved into two components, CS of the type $\frac{1}{2}[0\bar{1}1]$ (121) for removal of oxygen planes, and antiphase boundaries, $\frac{1}{2}[0\bar{1}1]$ (011), for "stress relief." The concept of "stress relief" in the present case is similar to this, although production of true antiphase boundaries with cation movement is not necessary. The driving force for "stress relief" subsequent to anion removal here arises out of the necessity to achieve an equilibrium, minimum energy configuration of vacancies or interstitials from the metastable distribution resulting from anion removal on the most reactive crystallographic planes. In this respect, anion removal by unit slip from these fluorite-related structures is analogous to Gado's (*7*) "precursor to shear" for elimination of anions prior to collapse and shear in the CS structures. The distinction between CS and "unit slip" mechanisms is, however, quite clear. If anions are removed along anion-only planes (e.g., $(111)_F$ in fluorite-type structures) structure collapse and CS can occur. Elimination of anions from planes across which collapse cannot take place, can only be described by a "unit slip" or similar mechanism. As stated earlier, any reaction mechanism such as "unit slip" can, at this stage, only be proposed tentatively and other reaction mechanisms for the form-

ation of defect structures in fluorite-related systems are, or course, possible. "Unit slip" provides a rational explanation for all of the observations of the present series of experiments. Clearly, further experiments, particularly observation and analysis of dislocations similar to those performed on UO_2 and LaF_3 (*27*), need to be done. Implicit in this last statement is the assumption that the rates of the pyrohydrolysis reactions can be suitably controlled and that the crystal defects produced by them (sublattice dislocations) can be meaningfully observed.

References

1. B. G. HYDE, L. A. BURSILL, M. O'KEEFFE, AND S. ANDERSSON, *Nature (London)* **237**, 35 (1972).
2. B. G. HYDE, *Acta Cryst.* **A27**, 617 (1971).
3. J. G. ALLPRESS AND A. D. WADSLEY, *J. Solid State Chem.* **1**, 28 (1969).
4. L. A. BURSILL AND B. G. HYDE, *Phil. Mag.* **20**, 657 (1969).
5. L. A. BURSILL AND B. G. HYDE, *Phil. Mag.* **23**, 3 (1971).
6. L. A. BURSILL, B. G. HYDE, AND D. K. PHILP, *Phil. Mag.* **23**, 1501 (1971).
7. P. GADÓ, *Acta Phys. Hung.* **18**, 111 (1965).
8. J. S. ANDERSON AND B. G. HYDE, *Bull. Soc. Chim. France* p. 1215 (1965).
9. J. S. ANDERSON AND B. G. HYDE, *J. Phys. Chem. Solids* **28**, 1393 (1967).
10. S. ANDERSSON AND A. D. WADSLEY, *Nature (London)* **211**, 581 (1966).
11. B. G. HYDE, D. J. M. BEVAN, AND L. EYRING, *Phil. Trans. Roy. Soc.* **A259**, 583 (1966).
12. D. J. M. BEVAN, *J. Inorg. Nucl. Chem.* **1**, 49 (1955).
13. M. R. THORNBER, D. J. M. BEVAN, AND E. SUMMERVILLE, *J. Solid State Chem.* **1**, 545 (1970).
14. B. T. M. WILLIS, *J. Phys.* **25**, 431 (1964).
15. W. H. ZACHARIASEN, *Acta Cryst.* **4**, 231 (1951).
16. A. W. MANN AND D. J. M. BEVAN, *J. Solid State Chem.* **5**, 410 (1972).
17. U. ROETHER, Ph.D. Thesis, Albert Ludwig's Universität zu Freiburg im Briesgau (1967).
18. A. W. MANN AND D. J. M. BEVAN, *Acta Cryst.* **26**, 2129 (1970).
19. A. R. MOLYNEUX, Ph.D. Thesis, The Flinders University of South Australia (1973).
20. M. G. PATON AND E. N. MASLEN, *Acta Crys.* **19**, 307 (1965).
21. R. GRAHAM, B.Sc. Hons. Thesis, The Flinders University of South Australia (1971).
22. B. G. HYDE, Private communication.
23. A. W. MANN AND D. J. M. BEVAN, *Acta Cryst.* to be published.
24. L. EYRING AND B. HOLMBERG, "Nonstoichiometric Compounds," p. 55, Amer. Chem. Soc. Publ. (1963).
25. F. R. N. NABARRO, "Theory of Crystal Dislocations," p. 231, Oxford University Press (1967).
26. W. A. BRANTLEY AND Ch. L. BAUER, *Phys. Status Solidi* **40**, 707 (1970).
27. K. H. G. ASHBEE, "The Chemistry of Extended Defects in Non-Metallic Solids," p. 323, North Holland (1970).